Microbiological influences on fracture surfaces of intact mudstone and the implications for geological disposal of radioactive waste

H Harrison[1]*, D Wagner[1], H Yoshikawa[2], J M West[1], A E Milodowski[1], Y. Sasaki[2], G Turner[1], A Lacinska[1], S Holyoake[1], J Harrington[1], D Noy[1], P Coombs[1], K Bateman[1] and K Aoki[3]

[1]British Geological Survey, Keyworth, Nottingham NG12 5GG, UK

[2]Japan Atomic Energy Agency (JAEA), Muramatsu 4-33, Tokai-mura, 319-1194 Ibaraki, Japan

[3]Japan Atomic Energy Agency (JAEA), 2-432 Hokushin Horonobe-cho, Teshio-gun, Hokkaido, 098-3224 Japan

*Corresponding author email: hmh@bgs.ac.uk

Abstract

The significance of the potential impacts of microbial activity on the transport properties of host rocks for geological repositories is an area of active research. Most recent work has focussed on granitic environments. This paper describes pilot studies investigating changes in transport properties that are because of microbial activity in sedimentary rock environments in northern Japan. For the first time, these short experiments (39 days maximum) have shown that the denitrifying bacteria, *Pseudomonas denitrificans,* can survive and thrive when injected into flow-through column experiments containing fractured diatomaceous mudstone material and synthetic groundwater under pressurised conditions. Although there were few significant changes in the fluid chemistry, changes in the

permeability of the biotic column were quantitatively monitored. These same methodologies could also be adapted to obtain information from cores originating from a variety of geological environments including oil reservoirs, aquifers and toxic waste disposal sites to provide an understanding of the impact of microbial activity on the transport of a range of solutes, such as groundwater contaminants and gases (e.g. injected carbon dioxide).

Introduction

Risk assessments for geological repositories for radioactive waste are based primarily on the precepts of contaminant transport, and are concerned with understanding the movement of gas, water and solutes through engineered barriers and natural groundwater systems, within the source-pathway-receptor paradigm. The emphasis on solute transport is particularly important in the development of theoretical models. However, it is well recognised that microbes live in a wide range of subsurface environments (e.g. West and Chilton, 1997; D'Hondt *et al.*, 2002; Lin *et al.*, 2006) including potential geological repository host rocks (e.g. West *et al.*, 1982; West 1995; Pedersen 1999; West and McKinley 2002; Keith-Loach and Livens 2002; Humphreys *et al.*, 2009); and their presence can have an impact on transport processes (Fredrickson *et al.*, 1989; Cunningham *et al.*, 1997; West and Chilton 1997; Chapelle 2000; Keith-Loach and Livens 2002; Coombs *et al.*, 2010). Microbial activity in any environment is located on chemical or physical interfaces, usually within biofilms and their impact on transport can be physical (e.g. altering porosity) and/or chemical (e.g. changing redox conditions or altering pH) often resulting in

intracellular or extracellular mineral formation or degradation (Milodowski *et al*., 1990; Beveridge *et al*., 1997; Konhauser *et al*., 1998; Ehrlich 1999; Tuck *et al*., 2006; Konhauser 2007). Consequently, the significance of microbial activity on the transport properties of potential host rocks for geological repositories is now being investigated (e.g. Pedersen 1999; Ferris *et al*., 1999; Hama *et al*., 2001; Vaughan *et al*., 2001; Brydie *et al*., 2005; Anderson *et al*., 2006; Tuck *et al*., 2006; Coombs *et al*., 2008). Most of this work has focussed on granitic environments that are potential hosts for *nuclear waste repositories*. This paper will describe recent work investigating changes in transport properties in sedimentary (mudstone) rock environments in northern Japan.

Geological Background

The Japan Atomic Energy Agency (JAEA) is constructing an underground research laboratory (URL) at Horonobe in northern Hokkaido to carry out research on the feasibility and safety of deep geological disposal.

The Horonobe site is located in north-western Hokkaido, about 50 km south of Wakkanai, and the geological setting of the URL has been summarised by Milodowski *et al*., (2004). It is located on a low-lying coastal plain of Quaternary alluvial and terrace deposits resting on Neogene (Tertiary) rocks. The Neogene strata comprise a thick sequence of marine sandstones, mudstones and shales deposited within the Mesozoic Tempoku Basin. The onshore part of this basin extends north-south in the northern district of Hokkaido, and is filled by a sequence of Cretaceous to Tertiary sedimentary rocks (Waseda *et al*., 1996). In the Horonobe area, the strata dip steeply to

the west with a north-westerly strike. There are several large faults, which generally trend northwest–southeast. One of these, the Horonobe Fault to the east of the area, is the major structure that delineates the eastern margin of the onshore Tempoku Basin.

The Horonobe site is underlain by Neogene strata. The sedimentary sequence passes upwards from Wakkanai Formation (massive siliceous diatomaceous mudstones including opal-CT), through the Koetoi Formation (massive diatomaceous mudstones including opal-A, but not opal-CT) to the Yuchi Formation (fine to medium grained sandstones) and to the Sarabetsu Formation (alternating beds of conglomerate, sandstone and mudstone, intercalated with coal seams) which is overlain by late Pleistocene to Holocene deposits (Ishii *et al.,* 2010).

The Tempoku Basin contains several north-south trending en-echelon anticlinal structures. A number of oil and gas fields were discovered within these structures between 1915 and 1942. The reservoirs are mainly sandstones in the Miocene Masuporo Formation and, to a lesser extent, sandstones in the Wakkanai and Koetoi Formations. The hydrocarbons were sourced from the organic rich shales and mudstones of the deeply-buried Wakkanai and Masuporo Formations. The reserves were very small; production ceased by 1970, with the exception of the Toyotomi Field (about 10-15 km north of Horonobe), which was still a producing gas field in 1996 (Waseda *et al*., 1996).

Geomicrobiology of Horonobe

Geomicrobiological assessments of ground waters, from boreholes previously constructed at Horonobe, have revealed the presence of a diverse indigenous microbiological ecosystem (e.g. Aoki *et al*., 2003; Kato *et al*., 2009). The impacts of the presence of these microbes on the performance of a high-level radioactive waste (HLW) repository, using geomicrobiological data from Horonobe, is being evaluated using a numerical code (Tochigi *et al.,* 2007). This code models biochemistry and geochemical equilibrium considering solute transport and microbial activity of specific microbial groups classified by their metabolism as 'aerobic', 'denitrifying', 'manganese reducing', 'iron reducing', 'sulphate reducing' and 'methanogenic'. Using groundwater information from Horonobe, Tochigi *et al*., (2007) have shown that denitrifying bacteria is likely to be the group of organisms with the greatest activity. Consequently, the impact of this group of organisms on Horonobe rock transport properties is the focus of the current study.

Laboratory techniques

The aim of the study was to evaluate how biofilms, generated by denitrifying soil bacteria *Pseudomonas denitrificans*, influenced the flow of synthetic Horonobe groundwater through fractured Horonobe mudstone. Two experiments, one biotic and the other an abiotic control, were carried out using a flow-through column operated at a constant rate of fluid flow and under pressurised conditions. Changes in biological and chemical parameters were monitored throughout the experiment together with

changes in confining pressure and temperature. The experiments were short-term pilot studies (maximum of 39 days) and conducted using diatomaceous mudstone material of the Koetoi formation taken at 40 m and 90 m depth. A matrix-matched artificial groundwater, based on the chemical composition of naturally occurring groundwater at Horonobe was prepared and supplemented with sodium acetate (0.25 g l^{-1}), to provide a readily available source of organic carbon to sustain bacterial growth (Table 1). The artificial groundwater was sterilised by filtration though a filter (0.2 μm). The addition of sodium acetate was necessary to promote microbial activity as this pilot experiment was short-term. Initially, this would exaggerate biogeochemical activity. However, over an extended period of time, indigenous bacteria were expected to utilise the naturally occurring DOC as geochemical analysis showed the organic content of the rock to be quite high. A full description of all methodologies is given elsewhere (Harrison *et al*., 2010).

Flow-through column experiment methodology

The flow-through column experiments were performed using intact Horonobe rock core, containing naturally occurring longitudinal fractures. Core material was positioned vertically in a Teflon sheath with end caps allowing fluid flow through the column and the assembly was then placed in a pressure vessel. Schematics of the completed experimental rig with the pressure vessel and rock core assembly are shown in Figures 1 and 2.

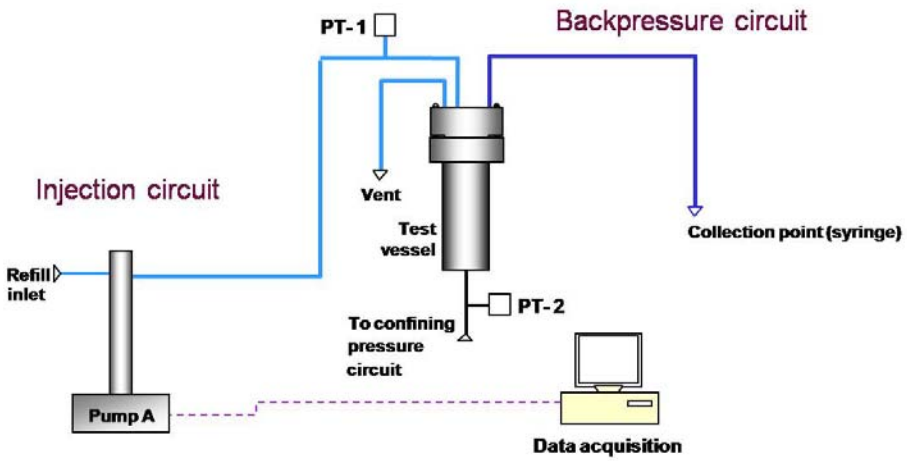

Figure 1 Schematic of column design.

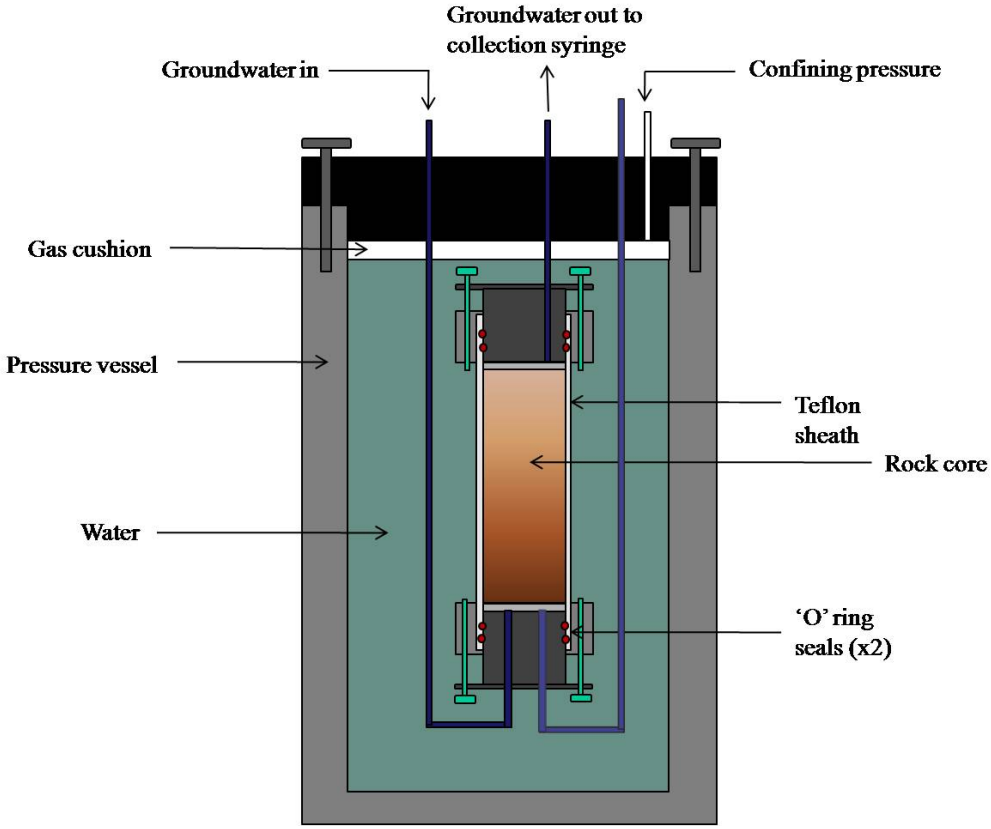

Figure 2 Schematic of pressure vessel with column containing rock core

Once assembled, the pressure vessel was partially filled with deionised water and pressurised to 1250-1260 kPa. The synthetic Horonobe groundwater was used to fill the syringe pump and the flow rate was set at 300 µl hr^{-1} (~ 7.2 ml day^{-1}). The cores were not pre-saturated with artificial groundwater prior to the start of the experiment. The first 'biotic' column

was injected with *P. denitrificans* after 11 days and the test was terminated after 39 days in total. The second 'abiotic' column was not injected with the organisms and the test was terminated after 31 days.

Pressure transducers, shown in Figure 1 as PT 1 and PT 2, were used to monitor the pressure changes within the cores while the syringe pumps controlled the flow-rate. The transducer outputs were recorded, along with actual pressure measurements on a calibrated DRUCK DPI 610 pressure calibrator and these data were used subsequently to calibrate the pumps and transducers. Other variables (e.g. vessel temperature, air temperature and confining pressure) were also logged continuously during the course of the experiment. Fluid samples were collected by syringe at regular intervals for chemical and biological analyses.

Preparation of the intact core material

Two cores were taken at depths of 40.80–41.00 m and 90.04-90.24 m respectively, from boreholes drilled at a downward inclination of 41° from the drift wall at the depth of 140 m. The cores were covered in protective wax and shipped from Japan by courier. On receipt, physical parameters, e.g. overall dimensions, orientation at sampling, location of fractures and other imperfections were recorded for each core before reference samples were taken for the mineralogical characterisation. The cores were re-drilled to produce a fresh surface and reduce the possibility of contamination from the original drilling fluids; each core was then cut using a saw to a suitable length to fit into the column assembly. The material sampled at 40 m depth was used for the biotic experiment as it had a naturally occurring

longitudinal fracture. The 90 m material was used for the abiotic test, visually it did not appear to be fractured but once subjected to a sharp impact its friability gave rise to multiple longitudinal fracture surfaces. The orientation of the cores at sampling was reproduced when the material was loaded into the test rig.

Preparation of the bacterial culture

A freeze-dried culture was received from National Collection of Industrial, food and Marine Bacteria (NCIMB), UK. The strain used was *Pseudomonas denitrificans* (NCIMB 9496). Resuscitation of the bacteria took place in a recommended growth media of nutrient broth, CM0001 (Oxoid), which was incubated at 25ºC.

To prepare the cultures for inoculation, the active cultures were transferred to sterile 35 ml centrifuge tubes and centrifuged at 4600 rpm for 10 minutes. The supernatant was removed from each tube using sterile disposable pipettes and replaced with sterile synthetic groundwater. This process was repeated a further four times to ensure traces of the growth media were removed. Decreasing volumes of synthetic groundwater were added at each stage to concentrate the bacteria. The resulting fluid was then added to approximately 500 ml of synthetic groundwater, this produced sufficient volume to fill the syringe pump. A 1 ml sample of each suspended culture was removed by sterile pipette and preserved in gluteraldehyde fixative solution (Jass and Lappin-Scott, 1992) prior to microscopic examination. The total number of bacteria inoculated was then determined by direct

counting using epifluorescence microscopy (Hobbie *et al*., 1977; Jass and Lappin-Scott, 1992).

Chemical analyses

A reference sample of the artificial groundwater used to fill the syringe pump was taken for comparison to the outflow fluids from the biotic and abiotic columns at the start of each test (day 0) and at 7 day intervals until the end of the experiments. Chemical analyses included major anions by ion chromatography, (IC) and cations by Inductively Coupled Plasma - Optical Emission Spectroscopy, (ICP-OES), as well as redox sensitive species (Fe^{2+}/Fe^{3+}), pH and selected microbial nutrients (e.g. C, P, S and N). Non-Purgeable Organic Carbon (NPOC) was also evaluated which gives an indication of the degradation rate of organic compounds during the experiments.

Microbiological analyses

Microbial biomass was evaluated using epifluorescence microscopy. Epifluorescence microscopy uses a short wavelength transmission source to fluoresce a sample stained with the nucleic acid selective cationic fluorochrome. The fluorescent stain, Acridine Orange, or N,N,N',N'-tetramethylacridine-3,6-diamine ($C_{17}H_{19}N_3$), was used to determine total cell counts (Hobbie *et al*., 1977; Jass and Lappin-Scott, 1992). Acridine Orange is capable of permeating cells and interacting with DNA and RNA by intercalation or electrostatic attractions. When the fluorescent stain, which is spectrally similar to fluorescein, interacts with DNA, the excitation maximum is at 502 nm (cyan) and the emission maximum at 525 nm

(green), while RNA interactions shift the excitation maximum to 460 nm (blue) and the emission maximum to 650 nm (red). Thus, it is possible to determine if cells are metabolically active as they appear red due to the predominant RNA whereas inactive or slow growing bacteria have mostly DNA and appear green. By examination of 20 randomly selected fields of view, the numbers of bacteria per ml can be counted.

Mineralogical analyses

Quantitative X-Ray diffraction

Bulk mineralogical analysis was carried out on the original Horonobe cores (40 m and 90 m) and on the post-experimental residues (biotic and abiotic) by X-ray diffraction (XRD) analysis using bulk-powdered samples. Material for XRD analysis was prepared as randomly orientated sample mounts. The principal mineralogical components were identified by comparison to reference diffraction data, and then quantified (for components other than clay minerals) by computer modelling the XRD diffraction profiles using the Rietveld refinement technique (Snyder and Bish, 1989). The clay mineralogy was characterised by XRD analysis of the <2 μm fraction, which was separated from the disaggregated bulk rock material by dispersion in water and the <2 μm fraction collected following differential sedimentation according to Stoke's Law. XRD analysis was carried out using a PANalytical X'Pert Pro series diffractometer equipped with a cobalt-target tube, X'Celerator detector and operated at 45 kV and 40 mA. Diffraction data were initially analysed using PANalytical X'Pert Highscore

Plus version 2.2a software coupled to the latest version of the International Centre for Diffraction Data (ICDD) database.

BET Surface area analysis

BET surface area analysis was performed on crushed original core samples (40 m and 90 m) and the post-experimental residues (biotic and abiotic) using a Micromeritics Gemini VI surface area analyser. Surface area analyses were carried out using the multipoint BET/N2 method based on the quantity of gas that adsorbs as a single layer of molecules on a solid surface.

Petrographic analysis

The morphological characteristics and mineralogy of the fracture surfaces in the pre- and post-experimental core materials were examined initially by optical binocular microscope and then examined in detail by cryogenic (cryoSEM), variable pressure (VPSEM) and environmental (ESEM) scanning electron microscopy (SEM) techniques. SEM analyses were performed using a FEI Company QUANTA 600 environmental scanning electron microscope INCA and a LEO 435VP variable pressure scanning electron microscope. SEM observations were recorded using electron beam accelerating voltages of 10-20 kV and probe currents of 0.8-2 pA (FEI QUANTA 600) and 100-500 pA (LEO 435VP). Mineral identification was aided by semi-quantitative microchemical observations recorded using energy-dispersive X-ray microanalysis (EDXA) that was carried out simultaneously during SEM observation. EDXA analyses were performed using either: an Oxford Instruments INCA Energy 450 EDXA system with a 50 mm^2 silicon drift detector (SSD) fitted to the FEI QUANTA 600 ESEM;

or an INCA Energy 450 EDXA system with a thin window SiLi X-ray detector fitted to the LEO 435VP SEM.

SEM analysis of the starting material was carried out on uncoated, dried subsamples of fracture surface, using VPSEM and backscattered electron imaging (BSEM) on the LEO 435VP SEM instrument. Samples of wet reacted fracture surface were initially examined as uncoated, frozen samples by cryoSEM using BSEM on the LEO 435VP instrument. High-resolution morphological observations were carried out on the FEI QUANTA 600 ESEM instrument, using environmental secondary electron imaging of uncoated moist samples under ESEM mode, and by cryoSEM of gold-coated frozen samples under high vacuum mode.

SEM analysis of starting material

A subsample of starting core material used in the flow-through column experiment was carefully prised open to expose a fresh fracture surface. A small piece (approximately 20 x 20 mm), was broken and mounted onto a 25 mm diameter aluminium SEM stub using Leit-C conductive-carbon-cement. This was examined directly in VPSEM and imaged by BSEM. The BSEM images provide some morphological information but also discriminate the different mineral/phases in relation to the density and average atomic number of the phase being imaged (Goldstein *et al*., 1981).

SEM analysis of reacted material

The reacted core samples from both experiments were photographed immediately after recovery from the experimental cell. The core readily

parted along the steeply inclined fracture and the fracture surfaces were then examined by SEM. CryoSEM was carried out within 2 hours of opening the core sample. However, in order to prevent the sample drying out prior to cryoSEM and VPSEM analysis the material was stored, suspended above water, in a sealed vessel maintained at 5°C in a refrigerator.

For cryoSEM analysis, approximately 5 x 5 x 5 mm fragments of moist sample containing part of the fracture surface were carefully prised from the parent sample using a fine chisel and lightweight hammer. These fragments were mounted onto a gold-plated cryogenic sample carrier. The samples were held in place on the sample carrier either by small steel "jaw-clip" fixed to the carrier, or by using a small drop of cryogenic mounting compound (Tissue-Tek® O.C.T™ Compound - carbowax in polyvinyl alcohol solution). This ensured good thermal contact on the cryogenic sample carrier. The mounted sample was rapidly pre-frozen by immersion in a melting mixture of solid and liquid nitrogen "slush" and then transferred under vacuum onto a cold nitrogen gas-cooled SEM cold-stage.

The SEM cold-stage was initially maintained at a temperature of approximately -170°. The surface of the sample was then "developed" by warming to approximately -80°C and slowly ablating the frozen porewater from the surface of the sample, to reveal the underlying fabric of the frozen rock surface. After achieving the required level of detail by ablating the ice, the sample was rapidly re-cooled to -170°C to stop further ablation. The cryogenic samples were examined in the LEO 435VP SEM instrument by BSEM imaging of uncoated material, using a low pressure (0.3 to 0.4 torr) nitrogen gas atmosphere. Higher-resolution cryoSEM observation of the

fracture surfaces were recorded using the FEI QUANTA 600 ESEM instrument. The fracture surfaces were initially observed uncoated, using the ESEM instrument under high vacuum conditions (<2 x 10^{-4} torr). The cryogenic samples were then gold-coated after ablation by vacuum gold-sputter coating in the on-column cryogenic sample preparation chamber, and re-examined under cryoSEM operation.

High-resolution secondary electron imaging of moist subsamples of the fracture surfaces from the reacted cores was also undertaken using the ESEM instrument. Approximately 20 x 10 x 5 mm fragments of the undisturbed fracture surface were mounted directly onto the ESEM sample stage using a small piece of Plasticine® to hold the sample in place. ESEM observations were recorded under a water vapour atmosphere at a pressure of 0.4 to 0.5 torr.

Physical measurement results

Both biotic and abiotic experiments were performed at a constant flow rate and changes in injection and confining pressure were continuously logged by pressure transducers during the tests. These are depicted graphically in Figure 3 (biotic experiment) and Figure 4 (abiotic control experiment).

Biotic column experiment

Sterile artificial groundwater was pumped through the core assembly for a nominal period (11 days) before the *P. denitrificans* bacteria were injected. The pump was stopped, which caused a brief dip in pressure (Figure 3) and the sterile water was replaced with 500 ml of water inoculated with the

bacteria. The pump was restarted and the experiment was terminated after 39 days.

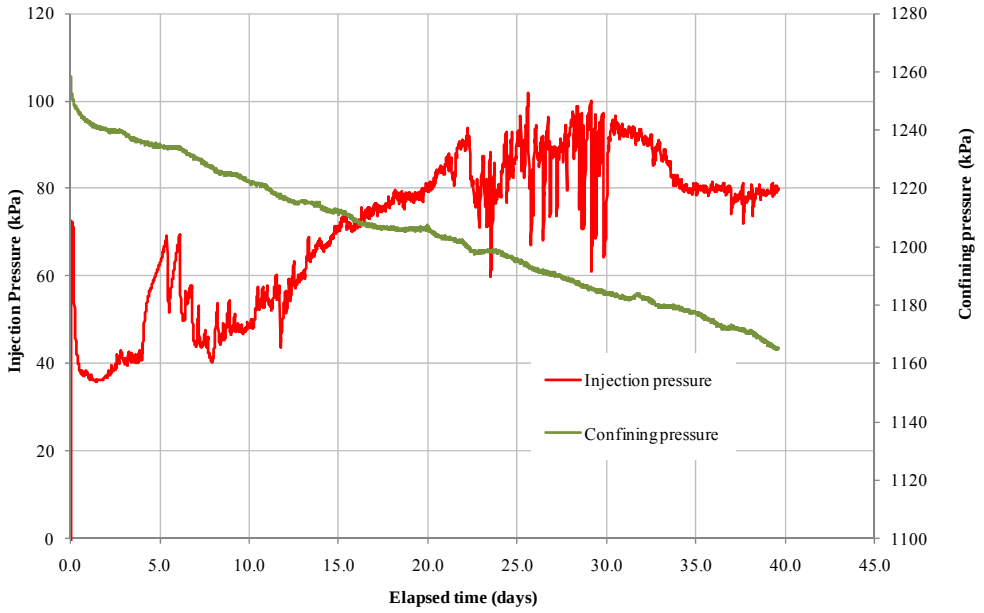

Figure 3 Biotic experiment: injection and confining pressure data plotted against experiment duration in days

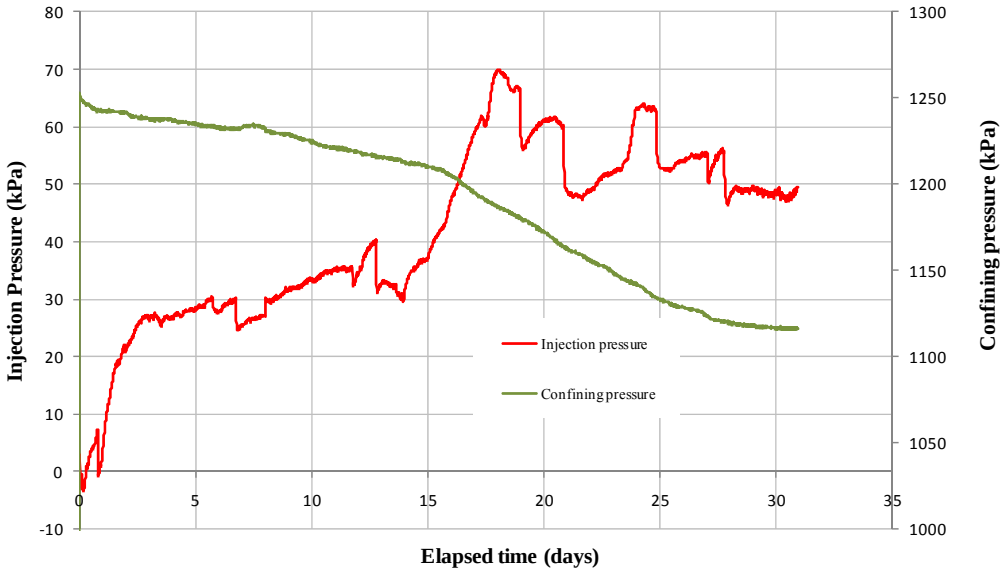

Figure 4 Abiotic experiment: injection and confining pressure data plotted against experiment duration in days

At the start of the experiment a sharp increase in injection pressure was observed starting at 41 kPa (3.9 days) and rising to 69 kPa (5.3 days). At 5.5 days, the pressure decreases rapidly to 50 kPa. This pattern in the pressure profile occurred a second time when a maximum of 69 kPa was reached at 6 days before decreasing to 51 kPa at 6.3 days. As the bacteria were not injected until 11 days, changes in the permeability of the core may have been caused by the movement of fines. Blocking of the pore spaces by fine grained material would cause a localised increase in pressure and since the flow was maintained at a constant rate, breakthrough would occur as the pressure rose and new pathways were established. The pressure profile showed a gradual but steady increase from day 8 to day 23, although a dip was observed when the bacteria are injected at day 11. From day 23 to 30, the pressure averages around 88 KPa. However, the intermittent pressure 'spikes' observed at this time may have been the result of either transducer noise or further substantial changes in flow geometry. Due to the fracture, the material was highly permeable (i.e. the pressure within the core was low) and the pressure changes observed fell within the specified noise tolerance of the transducers. Transducer noise is caused by a poor electrical connection and is generally recorded as rapidly occurring spikes in the pressure data log. However, in this experiment, quiescent periods in the data were bracketed by pressure maxima and minima spanning time periods of several hours. In addition, this pressure pattern was only observed in the biotic core. It was therefore more likely to be the result of microbial activity causing partial blocking of the pore spaces with biological material. From day 30 to day 35, a gradual decrease in pressure was observed. From 35

days onwards the transducer response showed signs of a stabilisation in pressure of 80 kPa, thereafter the system began to oscillate in a quasi-steady state. The term quasi-steady describes a system where some parameters are fluctuating or not fully evolved but is close to achieving a steady state (a condition where all the variables remain constant and unchanging over time).

Overall, the short but rapid changes in pressure could be explained by partial clogging of conductive pathways either by fines, biofilm or a combination of both, which were then flushed as the hydraulic pressure locally increased. The resultant saw-tooth like pressure profile observed in the biotic core during the experiment was symptomatic of a dynamic system exhibiting localised intermittent changes in permeability.

Abiotic column experiment

The abiotic column experiment ran for 31 days in total with no injection of organisms. As with the biotic experiment, pressure changes were continuously monitored throughout the course of the test.

Figure 4 shows that the maximum pressure achieved within the abiotic core was 70 kPa at 18 days; this was marginally lower than the biotic core which achieved a maximum of 102 kPa at 25.6 days. A gradual increase in pressure was observed in the abiotic core between 0 and 3 days, followed by an inflection in the pressure curve and a reduction in the rate of pressure change. From 3 days to 15 days the transducer response showed signs of a pressure stabilisation at around 32 ± 5 kPa. From 15 days onwards, the resistance to flow spontaneously increases which may be caused by either

localised blockages along conductive pathways or mechanisms associated with self-sealing, commonly observed in mud rocks (e.g. Cuss *et al*., 2006; Horseman *et al*., 2005). From 28 days onwards the transducer response showed signs of a pressure stabilisation at around 49 ± 3 kPa, thereafter the system again appears to begin to oscillate in a quasi-steady state.

The changes observed during the first three days of the abiotic column experiment may relate to the movement of water into pore spaces during the initial pressurisation of the system. The fact that this was not observed in the biotic core may have been due to differences in fracture geometry between the two test samples. The abiotic core was of higher permeability than the biotic core as it contained multiple fractures and this was shown by the considerably lower maximum pressure of 70 kPa achieved by the abiotic column system. The differences in pressure profiles between the two cores highlight the variability of such samples and the impact this may have on test results.

Several changes in pressure were observed during the course of the abiotic column experiment and despite most being within the noise of the pressure transducers, it was more likely to be the result of slow changes in flow geometry within the core giving rise to an overall change in permeability. From day 28 onwards, it was possible that the core was on the verge of achieving a quasi steady-state but this was not confirmed as the experiment ended on day 31.

Fluid measurement results

Microbiology

After 11 days, the sterile synthetic fluid injected into the 'biotic' column experiment was inoculated with $1.18x10^5$ ($8.88x10^3$ SE) bacteria ml^{-1} of *P. denitrificans.* The fluid was then passed through the core for a further 28 days. Samples of outflow fluid were taken at intervals and the mean numbers and standard error for total bacterial counts were determined by epifluorescence microscopy (Jass and Lappin-Scott, 1992) and given in Table 2. These show that no organisms were present in the outflow 7 days after injection but the numbers of organisms present in the outflow after 14 days was greater than those injected into the core. Thus the time for transit of the bacteria through the core is between 7 and 14 days. However, the numbers decline to $4.48x10^5$ bacteria ml^{-1} after 28 days, taking into account errors in measurement, this is still higher than the count at injection. To establish if the bacteria were still viable at the end of the experiment, the total bacterial counts of the fluid remaining in the syringe pump was also determined. The fluid was found to contain $6.48x10^8$ bacteria ml^{-1} (SE, $6.96x10^7$ bacteria ml^{-1}), of which 10% were considered to be viable. Results are only given for the biotic experiments as no bacteria were detected in the abiotic experiment.

Fluid chemistry

The detailed fluid chemistry analysis for the outlet fluids from the biotic and abiotic columns are given in detail elsewhere (Harrison *et al*., 2010). No significant differences were observed the chemistry of the outflow fluid

from the biotic column when compared to the abiotic column. This implies that the duration of each test may not have been long enough to allow chemical changes to be observed. Nevertheless, the concentrations of organic carbon (NPOC) decreased in the biotic core experiment from 62.5 mg l^{-1} (day 0) to 30.5 mg l^{-1} (11 days), the concentration then stabilised at ~30 mg l^{-1} until the end of the experiment (day 33). However, the addition of sodium acetate to initiate bacterial growth contributed 44 mg l^{-1} of organic carbon (NPOC) to the synthetic groundwater. It is interesting to note therefore that in the abiotic experiment the concentration of NPOC is three orders of magnitude greater than in the biotic and that this also reduces in concentration over the duration of the study from 6370 mg l^{-1} (day 0) to 4215 mg l^{-1} (day 30). This implies that the concentrations of NPOC vary greatly in the Horonobe core material.

Mineralogical results

Whole rock mineralogical analysis results

The results of whole-rock XRD analyses are summarised in Table 3 and labelled XRD traces are given elsewhere (Harrison *et al*., 2010).

The initial rock samples have similar mineralogies with major amounts of quartz (mean c. 39.8 %), albite (mean c. 19.8 %) and 'mica' (undifferentiated mica species possibly including muscovite, biotite, illite, illite/smectite etc.; mean c. 22.0 %) and minor/trace amounts of K-feldspar, 'kaolin' (one of the kaolin group minerals including halloysite, kaolinite etc.), chlorite, pyrite and smectite.

The sample traces obtained from XRD analyses also showed broad peaks between 20-35°2θ. Poorly ordered materials such as glasses or opaline silica species typically produce such broad features.

Halite was not detected in the starting material but was observed as a minor to trace component in both the biotic and abiotic reaction residues. This is an artefact of the sample preparation, and is derived from sodium chloride precipitated from the residual saline pore fluid during freeze-drying of the samples. In general, and taking into account the estimated errors in measurement, no evidence of any mineralogical changes in the sample due to bacterial interactions was observed in the experimental residue. The differences in clay mineral quantities that were observed between original sample core and the post-experimental biotic material may be due to bacterial interaction. However, this variation is more likely to be explained by sample heterogeneity and/or by the given quantification method where mineral concentrations below 3 wt.-% (Hillier *et al*., 2001) have given errors of typically ±40 %.

Clay mineral observations

XRD analysis of the <2 μm materials showed that the clay mineralogy of the starting materials was predominantly composed of illite and smectite and only small proportions of kaolinite and chlorite. Quartz and albite were also identified in the <2 μm fractions of the samples.

‘Non-swelling clays’

The non-swelling clays include illite, kaolinite and chlorite. Illite was identified by its characteristic air-dry d_{001} spacing of c.10.0Å which remains invariant after glycol-solvation and heating. Kaolinite was identified by its characteristic air-dry basal spacings of c.7.1 and 3.58Å which remain invariant after glycol-solvation but which disappear after heating at 550°C due to the meta-kaolinite’s X-ray amorphous state. Chlorite was identified by its characteristic air-dry and glycol-solvated basal spacing peaks at 14.2, 7.1, 4.73 and 3.54Å and particularly the presence of a peak at c.13.9Å after heating at 550°C.

‘Swelling clays’

The swelling clay smectite was identified by its typical air-dry d_{001} spacing of c.14.5Å which expands to a similarly typical c.17Å on glycol-solvation and collapses under heating to 550°C for 2 hours to an ‘illite-like’ 10Å d_{001} spacing.

BET surface area analysis

The results of BET/nitrogen surface area analyses are shown in Table 4. The original core samples have similar surface areas, c. 21.88 $m^2 g^{-1}$ at 40 m depth and c. 24.07 $m^2 g^{-1}$ at 90 m depth respectively.

Analyses of the post-experimental cores from both biotic and abiotic experiments did not show any significant change in surface area.

Optical and scanning electron microscopy observations

Starting material

Petrographical observation by VPSEM of the starting material showed that the surface of the steeply-inclined fracture running the length of the starting material was completely unmineralised. The rock was seen to be highly siliceous: composed largely of silt-sized fragments of diatoms with delicate microporous skeletal frameworks of silica, fine sand-grade siliceous cylindrical sponge spicule fragments. A proportion of the diatom detritus includes relatively complete cylindrical forms. Subordinate detrital components include angular silt-grade grains of quartz and irregular silt-grade aggregates of illitic clay. Minor detrital silt-grade angular grains of K-feldspar and plagioclase (probably of albitic to oligoclasic composition), and minor to trace muscovite were also present.

Fine grained authigenic pyrite was a significant component of the rock matrix, and fresh pyrite was also exposed in the fracture surface. The pyrite occurred either as framboidal aggregates in "clusters" or "pods" up to 100 μm diameter or as fine octahedral crystals (< 5 μm diameter) disseminated through the clay-silt-grade matrix (Figure 5). Minor siderite (magnesiosiderite ($[Mg,Fe]CO_3$) in composition) was also present as an authigenic phase. It occurred disseminated as small rhombs (up to 10 μm), and was found forming a replacive matrix cement lining the walls of burrow-like trace fossils. These burrow trace fossils were seen as diffuse pale grey to buff-coloured features in hand-specimen.

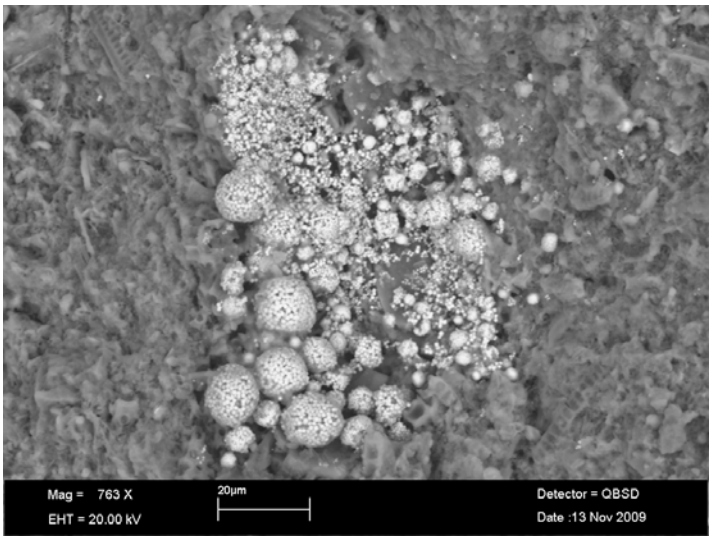

Figure 5 BSEM image (from VPSEM) showing framboidal aggregates of fine grained pyrite forming a discrete "pod" within the siliceous diatomaceous matrix. (Starting material). LEO 435VP SEM instrument.

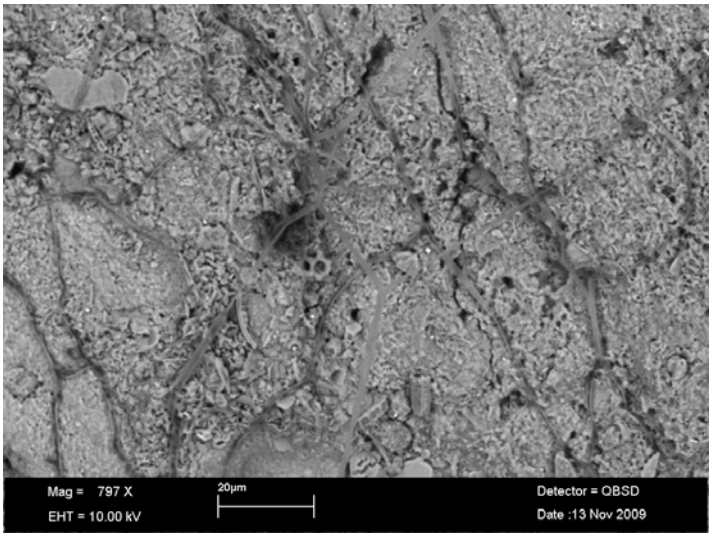

Figure 6 BSEM image (from VPSEM) showing network of fine organic filaments (possibly fungal hyphae) growing across the fracture surface, following and penetrating along the interconnected network of sub-parallel to anastomosing fine slickenside channels in the fracture plane. (Starting material). LEO 435VP SEM instrument

Detailed examination of the fracture surface revealed a series of fine-scale "ridge and furrow" lineation structures across the whole fracture surface. The morphology of these features, with aligned "crag" and "tail" slope surfaces suggests that these were probably features formed by shear-deformation parallel to the fracture surface (i.e. slickensides). VPSEM observations also showed that within these channels formed by the slickensides, loose silt particles were often present. Furthermore, fine organic filaments about 1-2 µm diameter were found to be present across

the whole fracture surface. These filaments formed an interconnected mesh and penetrated along the slickenside channels in the fracture surface (Figure 6 and Figure 7). No cellular structures were observed in the filaments and they appeared to have collapsed, possibly as a result of drying during sample preparation and under vacuum in the SEM instrument during VPSEM observation. In morphology, these features closely resembled fungal hyphal structures, although it was not possible to give a definite identification without further examination of intact core, which is beyond the remit of the current study.

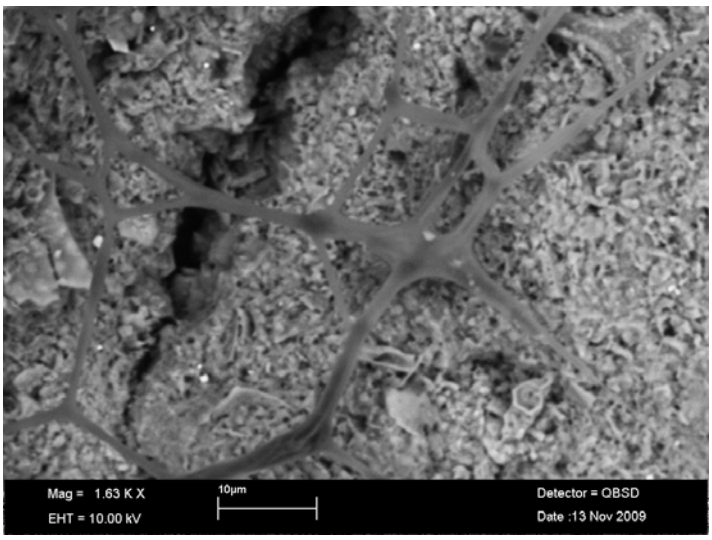

Figure 7 BSEM image (from VPSEM) showing detail of the fine organic filaments coating the fracture plane. (Starting material). LEO 435VP SEM instrument.

No evidence of mineralogical alteration of the fracture surface could be seen to be associated with these organic filaments. The surfaces of redox-sensitive minerals such as pyrite and siderite-magnesiosiderite were seen to be fresh and unaffected by oxidation products such as iron oxides or other alteration effects.

These observations clearly show that the starting material was already microbially contaminated and that fungi appear to be already in the fracture at the start of the experiment. These microbial features may have possibly been introduced after the initial drilling of the sample.

Biotic column experiment - post-experimental material

Observation of the core plug recovered after the completion of the biotic column experiment, inoculated with *P. denitrificans*, showed that there was small channel between the core and the heat-shrunk Teflon sheath, where a small fragment of one fracture wall had fallen away and was missing. Close examination of the surface of this "channel" feature showed that fine-grained mineral particles were "clotted" and bound together on the surface of the fracture by a gelatinous organic film.

On opening along the fracture plane, the fracture surfaces were seen to have a similar "ridge-and-furrow" surface morphology to that seen in the off-cut of the starting material. This indicates that these potential slickenside channels were extensively present across the whole of the fracture surface throughout the core sample.

Detailed cryoSEM observations show that, as in the starting material, the fracture surface was coated with organic biofilaments. These formed a dendritic meshwork across the fracture surface, and again, they followed and penetrated along the "channels" presented by the "ridge-and-furrow" morphological structures in the rock surface.

Closer examination of the filaments suggests that many of these filaments comprise “strings” of connected “rod-like” cells that were the expected size and morphology for bacterial cells (Figure 8). These cell-like structures were not observed in the starting material. However, it is not totally clear in all cases that the filaments are comprised of discrete cells, and some filaments are more similar to the filamentous structures seen in the starting material suggesting that both bacterial and fungal filaments were present.

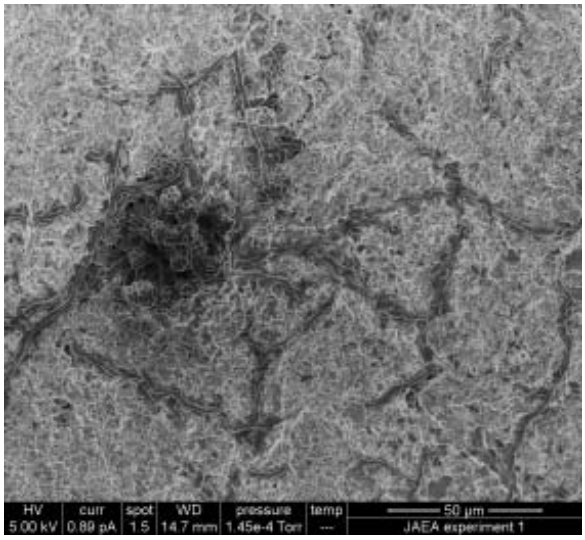

Figure 8 CryoSEM SEI image of the fracture surface showing clusters of cellular structures associated with biofilaments and showing that some biofilaments comprise strings of rod-like cells. Post-experimental material. (Biotic experiment). High vacuum cryoSEM, uncoated sample, FEI ESEM instrument.

The filamentous structures were also closely associated with isolated rod-like cells and clusters of cells (“bunches of grapes” aggregates) as seen in Figure 9. Isolated rod-like cells were clearly bacterial cells and probably represent discrete cells of denitrifying bacteria. It is not clear whether the clusters of rod-like cells and the strings and filaments are related. In some cases, the rods appeared to encase, and be living on, the surfaces of what appeared to be possible fungal filaments (Figure 10). In other cases, the

"bunches of grapes" aggregates may represent "fruiting" cells associated with parts of the filaments.

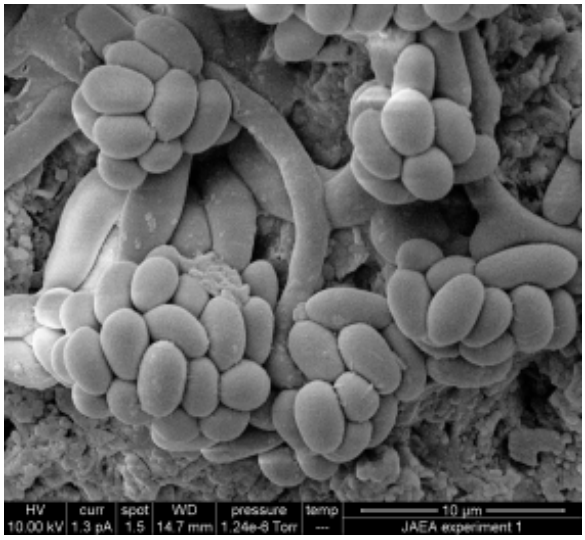

Figure 9 CryoSEM SEI image of the fracture surface showing detail of clusters of rod-like cells associated with biofilaments. Post-experimental material (Biotic Experiment). High vacuum cryoSEM, uncoated sample, FEI ESEM instrument.

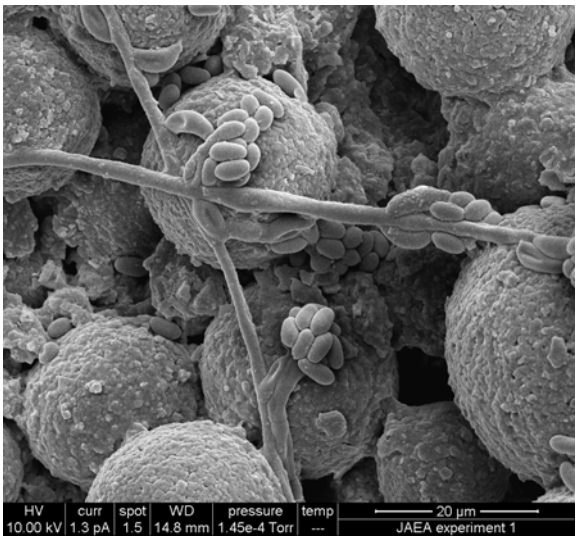

Figure 10 CryoSEM SEI image showing clusters rod-like cells associated with biofilaments resting on fresh framboidal pyrite. Post-experimental material. (Biotic experiment). High vacuum cryoSEM, gold coated sample, FEI ESEM instrument.

No obvious secondary mineralogical alteration products were observed on the fracture surface. The redox-sensitive minerals such as pyrite and magnesiosiderite were coated with microbial structures but showed no evidence of oxidation (Figure 10 and Figure 11). However, the biofilaments did appear to have caused some etching and dissolution mineral surfaces, affecting both pyrite and silicate substrates (Figure 11).

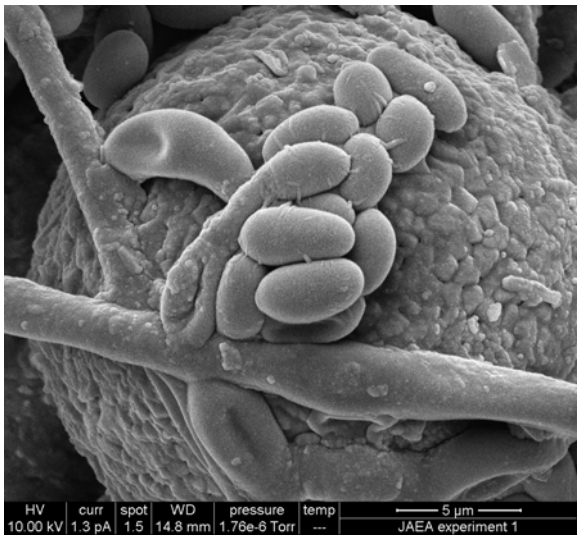

Figure 11 CryoSEM SEI image showing detail of the clusters rod-like cells associated with biofilaments resting on fresh framboidal pyrite. Fine pili structures can be seen on the rod-like cells that may function to bind the cell to mineral surfaces and adjacent cells. The pyrite appears to be unaffected by oxidation but the biofilaments can be seen to have etched into and are now embedded in the pyrite surface. Post-experimental material. (Biotic experiment). High vacuum cryoSEM, gold coated sample, FEI ESEM instrument.

Abiotic column experiment - post-experimental material

Detailed ESEM and VPSEM observations of the fracture surfaces found no evidence of any filamentous or other organic or biogenic structures similar to those found in the starting material and in the biotic column experiment. The surfaces of the fractures simply expose the host rock mineralogy

(Figure 12). Mineralogically, the fracture surfaces were similar to those described from the starting material and the biotic experiment.

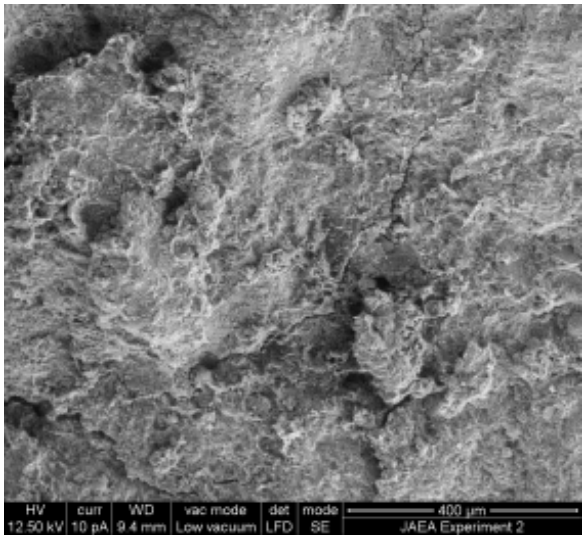

Figure 12 ESEM SEI image showing typical rough fracture wallrock surface devoid of any microbiological features. Post-experimental material. (Abiotic experiment). ESEM uncoated sample, FEI ESEM instrument

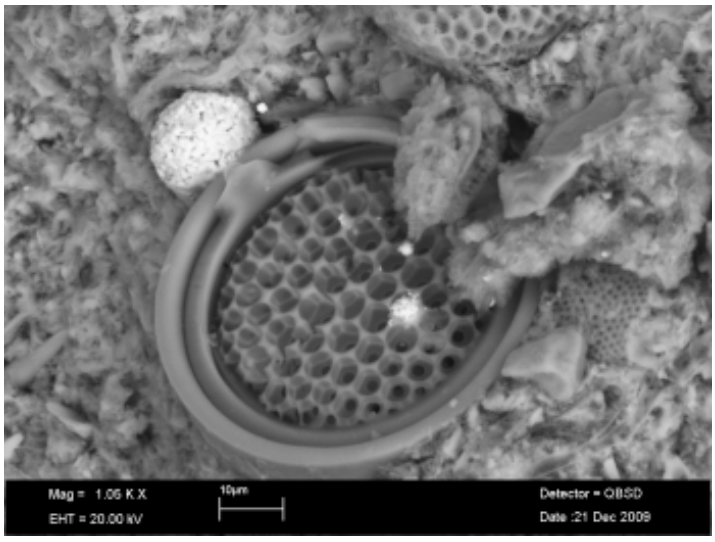

Figure 13 BSEM image of fracture wallrock showing fabric dominated by well-preserved silica diatom structures material and fine grained silica matrix comprised of finely comminuted diatomaceous debris. Well preserved diagenetic pyrite can be seen as framboidal aggregates and as fine pyrite locally replacing the diatom structres. Post-experimental material. (Abiotic experiment). VPSEM uncoated sample, LEO 435VP SEM instrument

The fracture surface mineralogy was dominated by biogenic silica derived from abundant fragments of siliceous diatom frustules and sponge spicules (Figure 13), with subordinate to minor clay minerals. The structure of the diatoms was extremely well-preserved and showed no evidence of alteration or dissolution during the experiment (Figure 13). Abundant authigenic pyrite was also present in the fracture surface occurring as framboidal aggregates. Disseminated and clusters of coarser octahedral crystals of authigenic pyrite, and fine pyrite partially replaced diatomaceous skeletons and detrital coalified woody plant fragments. Siderite was also present. Petrographical observations found no evidence for any mineralogical alteration: the authigenic pyrite and siderite were fresh with no evidence of oxidation and there was no evidence of dissolution or alteration of the siliceous and clay-rich matrix of the rock. No evidence was observed for the formation of any secondary mineral formation on the fracture surfaces.

Discussion

Both the biotic and abiotic column experiments were pilot studies of short duration (39 days maximum) although injection of bacteria into the biotic column experiment took place only over a period of 28 days. Nevertheless, the results show that *P. denitrificans* can survive under pressurised conditions for this period. Bacterial total numbers appear to increase from 1.18×10^5 (8.88×10^3 SE) bacteria ml^{-1} on injection to 4.48×10^5 (7.07×10^4 SE) bacteria ml^{-1} in the outflow fluid indicating that conditions are conducive to the growth and activity of this organism.

There were very few changes in the fluid chemistry in both the biotic and abiotic column experiments. This was due to the short duration of these pilot studies. However, chemical analysis showed that the concentrations of organic carbon (NPOC) varied greatly in the Horonobe core material.

Biological material was observed in the starting material and in post-experimental biotic material but not from post-experimental abiotic material. The structures observed in the biotic column experiment were significantly morphologically different to those seen in the starting material. Although it might be considered that some morphological differences could be attributed to differences in sample preparation – the starting material was examined as air-dried material and could have collapsed due to dehydration, whereas the biotic experiment material was examined in a moist or water-saturated state. However, there were clear morphological differences between the biogenic features seen in the starting material and the biotic experiment. The biogenic features seen in the biotic experiment included obvious clusters of cellular structures, isolated cells, and strings of cells of similar size to that expected for bacteria. Furthermore, these cells exhibited fine pili structures that are consistent with certain bacterial structures. In contrast, only fine organic filaments with no cellular structures were observed in the starting material. Filaments were also seen covering the fracture surface after completion of biotic column experiment. These filaments appeared to be different to those observed in the starting material. In many cases, the biotic column experiment biogenic filaments were closely associated with clusters of microbial cellular structures. In addition, some filaments appeared to consist of "strings" of elongate cells enclosed in

an organic film or mucilage, whereas this was not seen in the starting material. Finally, these filaments from the biotic experiment were observed to have locally etched the mineral substrate, and again this was not seen in the starting material. Similar biofilaments have been observed in other flow-through column experiments examining biofilm impacts on fluid transport through crushed diorite but under unpressurised conditions (Hama *et al*., 2001; Tuck *et al*., 2006; Coombs *et al*., 2008).

Therefore, it can be concluded that although the starting material had been affected by the activity of microbial contamination, this was completely different to the microbial effects seen in biotic column experiment. We interpret the microbial structures observed in the starting material as probable fungal filaments, produced by fungal degradation of the core samples after the cores were drilled. Potential microbiological contamination of sampled core is well recognised (e.g. Stroes-Gascoyne and West, 1996; Chapelle, 2000; Stroes-Gascoyne *et al*., 2007; Hallbeck and Pedersen, 2008; Polson *et al*., 2010) and the current study further illustrates this fact. However, the markedly different biological structures observed in the post-experimental biotic material were interpreted as a filamentous biofilm resulting from the activity of *P. denitrificans* introduced during the experiment. These filaments have utilised small microscopic channels in the fracture plane where tiny sub-parallel "ridges" and "troughs" formed as a result of shear along the fracture (i.e. slickensides) which create surface irregularities (or asperities) that do not fully interlock because of tiny displacement along the fracture surface. These represent potential fluid flow paths along the fracture. Similar microscopic channel-like fluid

transport pathways were also exploited by the growth of fungal contamination in the contaminated starting material.

Petrographical observations found no evidence for the oxidation of neither pyrite nor siderite in either the biotic experiment or the abiotic column experiment. In both cases, the pyrite surfaces were found to be fresh and free from any secondary iron oxide formation. In the biotic column experiment however, it was found that the microbial filaments had etched into the underlying rock substrate. The etching appeared to be non-specific with regard to surface mineralogy, affecting the silica-rich matrix, pyrite and siderite. No alteration or dissolution effects were observed in the starting material or in the abiotic column experiment. The interactions of microbes and minerals is long recognised (e.g. Beveridge *et al*., 1997; Ehrlich 1999; Konhauser *et al*., 1998; Milodowski *et al*., 1990; Tuck *et al*., 2006; Konhauser 2007) and past work has extensively demonstrated microbial dissolution of iron minerals such as pyrite and hematite, manganese and arsenic-bearing minerals and clay minerals (see reviews by Southam and Saunders 2005; Konhauser 2007; Shock, 2009). The current observations show that microbial etching of minerals in mudstones can also take place under pressurised conditions. However redox conditions were not controlled or monitored during these short-term experiments so the effect on mineral oxidation could not be fully evaluated.

Fluctuations in pressure within the cores were detected by the transducers during the biotic and abiotic column experiments. The pressure profile of the abiotic column showed small changes in permeability which could be the result of partial blocking of pore spaces by fines and the subsequent

flushing of material as new pathways were established. Overall, the pressure profile for the biotic column experiment followed a similar pattern to the flux observed in the abiotic column; however sharp 'spikes' were observed in the data between 23 and 30 days from the start of the biotic experiment. This feature could not be attributed to transducer noise as quiescent periods in the data were bracketed by pressure maxima and minima spanning time periods of several hours. As these sudden changes in pressure were only observed in the biotic column experiment, it was probably due to the formation of the observed biofilm. Previous unpressurised flow-through experiments with crushed diorite have also showed that biofilms influenced fluid flow (Hama *et al*., 2001; Tuck *et al*., 2006; Coombs *et al*., 2008).

Conclusions

- The results of these short-term pilot experiments have, for the first time, provided some insights into the influences of biofilms on fracture surfaces, which can be summarised as follows. Pseudomonas denitrificans can survive and thrive when injected into flow-through column experiments containing diatomaceous mudstone (Koetoi formation from Horonobe, Japan) and synthetic groundwater, supplemented with sodium acetate, under pressurised conditions. Microbially mediated changes in fractured cores can be detected using this technique. These same methodologies could also be adapted to obtain information from core from a variety of geological environments including oil reservoirs, aquifers and waste disposal sites to provide an understanding of the impact of microbial

activity on the transport of a range of solutes, such as groundwater contaminants and gases (e.g. injected carbon dioxide).

- Although there were few significant changes in the fluid chemistry, changes in the permeability of the core material in the columns were quantitatively monitored and the pressure profiles of the cores seem to indicate that microbial activity contributes to changes in fluid flow once biofilaments are established in the pore spaces.

- The pressure profiles are indicative of the material achieving a number of apparent quasi-steady states, suggesting highly dynamic and evolving systems. The distinctive 'spikes' observed in the pressure graph of the biotic core material were not seen in the abiotic experiment, and may only be explained by the observed biofilm formation.

- Due to the very short duration of the experiments, there was little time for extensive biofilm development. Nevertheless, the observations from the experiments have shown that biofilms from *P. denitrificans* do thrive over a 28 day period and that physical etching of minerals by biological material is occurring. Additionally, an effective methodology has now been developed to gain robust data in any future experiments.

- Minimal chemical information has been generated from these short-term column experiments which can be used in a computer model (Tochigi *et al.*, 2007). Longer duration experiments (i.e. over a period of a year or more) are needed to obtain such data which

would also yield information on the impacts of biofilms on fracture transport properties which is of great significance in understanding fluid movement in and around a repository. Long-term experiments will also allow equilibration of the experimental systems prior to injection of the perturbing organisms.

Acknowledgements

This paper is published with the permission of the Japan Atomic Energy Agency (JAEA) and the Executive Director of the British Geological Survey (NERC). The work forms part of the BGS 'BioTran' project and was partly funded by the Ministry of Economy, Trade and Industry of Japan (METI). We thank Ms Mai Kawagoe (Mitsubishi Corporation) for her assistance with the smooth running of the project.

References

Anderson, C., Pedersen, K. and Jakobsson, A. M. (2006) Autoradiographic comparisons of radionuclide adsorption between subsurface anaerobic biofilms and granitic host rocks. *Geomicrobiology Journal* **23**, 15-19.

Aoki, K., Kunimura, T., Hirota, Y. and Tazaki, K. (2003) Preliminary microbial analyses of groundwater in Horonobe Underground Research Laboratory, Hokkaido, Japan. Proc. *International Symposium on the Kanazawa University 21st Century Program* Vol **1**. Kanazawa University, Japan.

Beveridge, T. J., Makin, S. A. and Kadurugamuwa, J. L. & Li, Z. (1997) Interactions between biofilms and the environment. *FEMS Microbiology Reviews* **20**, 291-303.

Brydie, J. R., Wogelius, R. A., Merrifield, C. M., Boult, S., Gilbert, P., Allison, D. and Vaughan, D. J. (2005) The μ2M project on quantifying the effects of biofilm growth on hydraulic properties of natural porous media and on sorption equilibria: an overview. In: Shaw, R.A. (Editor). Understanding the micro to macro behaviour of rock-fluid systems. *Geological Society*, London. Special Publication **249**, 131-144.

Chapelle, F.H. (2000) *Ground-water microbiology and geochemistry*: New York, John Wiley and Sons, 468 pp.

Coombs, P., West, J. M., Wagner, D., Turner, G., Noy, D. J., Milodowski, A. E., Lacinska, A., Harrison, H. and Bateman, K. (2008) Influence of biofilms on transport of fluids in subsurface granitic environments – Some mineralogical and petrographical observations of materials from column experiments. *Mineralogical Magazine* **72,** 393-397.

Coombs, P., Wagner, D., Bateman, K., Harrison, H., Milodowski, A. E., Noy, D. and West, J. M. (2010). The role of biofilms in subsurface transport processes. *Q. J. Engineering Geology and Hydrogeology* **43**, 131-139.

Cunningham, A. L., Warwood, B., Sturman, P., Horrigan, K., James, G., Costerton, J. W. and Hiebert, R. (1997). Biofilm processes in porous media – practical applications. In: Amy, P.A., Haldeman, D. L. (eds), *The*

Microbiology of the Terrestrial Deep Subsurface. CRC Lews Publishers, pp 325-344.

Cuss, R.J., Reeves, H.J., Noy, D.J. and Harrington, J.F.(2006). Gas transport processes in argillaceous rocks within the EDZ: BGS contribution to NF-PRO WP4.4.1. *British Geological Survey Commissioned Report*, **CR/06/243**. 30pp.

D'Hondt, S., Rutherford, S. and Spivack, A. J. (2002) Metabolic activity of subsurface life in deep-sea sediments. *Science* **295**, 2067-2070.

Ehrlich, H. L. (1999) Microbes as geologic agents: their role in mineral formation. *Geomicrobiology Journal* **16**, 135-153.

Ferris, F.G., Konhauser, K.O., Lyvén, B. and Pedersen, K. (1999) Accumulation of metals by bacteriogenic iron oxides in a subterranean environment. *Geomicrobiology Journal*, **16**, 181-192.

Frederickson, J.K., Garland, T. R., Hicks. R. J., Thomas, J. M., Li, S. W. and McFadden, K. M. (1989) Lithotrophic and heterotrophic bacteria in deep subsurface sediments and their relation to sediment properties. *Geomicrobiology Journal* **7**, 53-66.

Goldstein, J. I., Newbury, D. E., Echlin, P., Joy, D. C., Fiori, C. and Lifshin, E. (1981) *Scanning Electron Microscopy and X-ray microanalysis*. Plenum Press, New York.

Hallbeck, L. and Pedersen, K. (2008) Characterisation of microbial processes in deep aquifers of the Fennoscandian Shield. *Applied Geochemistry*, **23**, 1796-1819.

Hama, K., Bateman, K., Coombs, P. Hards, V.L., Milodowski, A.E., West, J.M., Wetton, P.D., Yoshida, H., Aoki, K., (2001) Influence of bacteria on rock-water interaction and clay mineral formation in subsurface granitic environments. *Clay Minerals* **36**, 599-613.

Harrison, H., West, J. M., Milodowski, A. E., Bateman, K., Coombs, P., Harrington, J., Holyoake, S., Lacinska, A., Turner, G. and Wagner, D. (2010) Microbial influences on fracture surfaces of intact Horonobe mudstone (BioTran Progress Report Sept 2009 – January 2010). *British Geological Survey Report* ***OR/10/067***.

Hillier, S., Suzuki, K. and Cotter-Howells, J. (2001) Quantitative determination of Cerussite (lead carbonate) by X-ray powder diffraction and inferences for lead speciation and transport in stream sediments from a former lead mining area of Scotland. *Applied Geochemistry*, **16**, 597-608.

Hobbie, J. E., Daley, R. J. and Jasper, S. (1977) Use of nucleopore filters for counting bacteria by fluorescent microscopy. *Applied and Environmental Microbiology* **33**, 1225-1228.

Horseman, S.T., Cuss, R.J., Reeves, H.J., and Noy, D. (2005) Potential for self-healing of fractures in plastic clays and argillaceous rocks under repository conditions. *OECD Nuclear Energy Agency Report* **NEA-CC-3**, 351 pp.

Humphreys, P. N., West, J. M. and Metcalfe, R. (2009) Microbial effects on repository performance. *Technical Report QRS-1378Q-1*. Livelink reference number: 12208035. UK Nuclear Decommissioning Agency.

Ishii. E., Funaki, H., Tokiwa, T. and Ota, K. (2010) Relationship between fault growth mechanism and permeability variations with depth of siliceous mudstones in northern Hokkaido, Japan. *Journal of Structural Geology* **32**, 1792-1805.

Jass, J. and Lappin-Scott, H. M. (1992) *Practical course on biofilm formation using the modified Robbins Device.* University of Exeter.

Kato, K., Nagaosa, K., Kimura, H., Katsuyama, C., Hama, K., Kunimaru, T., Tsunogai, U. and Aoki, K. (2009) Unique distribution of deep groundwater bacteria constrained by geological setting. *Environmental Microbiology Reports* **1**, 569-574.

Keith-Roach, M. J. and Livens, F. R. (eds) (2002) *Interactions of microorganisms with radionuclides*. Elsevier, Oxford, UK. 400 pp.

Konhauser, K. O., Fisher, Q. J., Fyfe, W.S., Longstaff, F. J. & Powell, M. A. (1998) Authigenic mineralisation and detrital clay binding by freshwater biofilms: The Brahmani River, India. *Geomicrobiology Journal* **15**, 209-222.

Konhauser, K. O. (2007) *Introduction to Geomicrobiology*. Blackwell Science Ltd, Malden MA. USA. 425 pp.

Lin, L-H., Wang, P-L., Rumble, D., Lippmann-Pipke, J., Boice, E., Pratt, L. M., Sherwood Lollar, B., Brodie, E. L., Hazen, T. C., Andersen, G. L., DeSantis, T. Z., Moser, D. P., Kershaw, D. and Onstott, T. C. (2006) Long-term sustainability of a high-energy, low-diversity crustal biome. *Science* **314**, 479-482.

Milodowski. A. E., West, J. M., Pearce, J. M., Hyslop, E. K., Basham, I. R. and Hooker, P. J. (1990) Uranium-mineralised microorganisms associated with uraniferous hydrocarbons in southwest Scotland. *Nature* **347**, 465-467.

Milodowski, A. E. Barnes, R.P., Bouch, J., Kemp, S.J. and Wagner, D. (2004) Characterisation of fractured rock and fracture mineralisation in Horonobe Boreholes HDB-6, HDB-7 and HDB-8: Final Report. *British Geological Survey Report*, **CR/04/251**.

Pedersen, K. (1999) Subterranean microorganisms and radioactive waste disposal in Sweden. *Engineering Geology* **52**, 163-172.

Polson, E. J., Buckman, J. O., Bowen, D. G., Todd, A. C., Gow, M. M. and Cuthbert, S. J. (2010) An environmental scanning electron microscope investigation into the effect of biofilm on the wettability of quartz. *Society of Petroleum Engineers Journal* **15**, 223-227.

Shock, E. L. (2009) Minerals and energy sources for microorganisms. *Economic Geology* **104**, 1235-1248.

Snyder, R.L. and Bish, D.L. (1989) Quantitative analysis. In: Bish, D.L., Post, J.E. (Eds), Mineralogical Society of America, USA. *Modern Powder Diffraction, Reviews in Mineralogy* **20**, 101-144.

Southam, G., and Saunders, J. A. (2005) The geomicrobiology of ore deposits. *Economic Geology* **100**, 1067-1084.

Stroes-Gascoyne, S. and West, J. M. (1996) An overview of microbial research related to high-level nuclear waste disposal with emphasis on the

Canadian concept for the disposal of nuclear fuel waste. *Canadian Journal of Microbiology* **42**, 349-366.

Stroes-Gascoyne, S., Schippers, A., Schwyn, B., Poulain, S., Sergeant, C., Simanoff, M., Le Marrec, C., Altmann, S., Nagaoka, T., Mauclaire, L., McKenzie, J., Daumas, S., Vinsot, A., Beaucaire, C. and Matray, S-M. (2007) Microbial community analysis of Opalinus Clay drill core samples from the Mont Terri Underground Research Laboratory, Switzerland. *Geomicrobiology Journal* **24**, 1-17.

Tochigi, Y., Yoshikawa, H. and Yui, M. (2007) Modelling studies on microbial effects on groundwater chemistry. *Scientific Basis for Nuclear Waste Management XXX* **985**, 575-580.

Tuck, V. A., Edyvean, R. G.J., West, J. M., Bateman, K., Coombs, P., Milodowski, A. E. and McKervey, J. A. (2006) Biologically induced clay formation in subsurface granitic environments. *Journal of Geochemical Exploration* **90**, 123-133.

Vaughan, D.J., Wogelius, R., Boult S. and Merrifield, C. (2001) Quantifying the effects of biofilm growth on hydraulic properties and on sorption equilibrium microscopic to macroscopic measurements. *Progress summary 02/01 – 11/01 Williamson Research Centre, University of Manchester.*

Waseda, A., Kajiwara, Y., Nishita, H. and Iwano, H. (1996) Oil-Source Rock Correlation in the Tempoku Basin of Northern Hokkaido, Japan. *Organic Geochemistry*, **B24**, 351-362.

West, J. M., McKinley, I. G. and Chapman, N. A. (1982) Microbes in deep geological systems and their possible influence on radioactive waste disposal. In: *Radioactive Waste Management and the Nuclear Fuel Cycle,* **3**, 1-15.

West, J. M. (1995) A review of progress in the geomicrobiology of radioactive waste disposal. *Radioactive Waste Management and Environmental Restoration* **19**, 263-283.

West, J. M. and Chilton, P. J. (1997) Aquifers as environments for microbiological activity. *Quarterly Journal of Engineering Geology* **30**, 147-154.

West, J. M. and McKinley, I. G. (2002) The geomicrobiology of radioactive waste disposal. In: *Bitton, G. (ed) The Encyclopaedia of Environmental Microbiology*. John Wiley, New York, 2661-2674.

Table 1. Composition of synthetic groundwater

Reagent	**weight used (g l^{-1})**
NH_4Cl	0.6519
$NaHCO_3$	3.1528
$FeCl_3.6H_2O$	0.0133
KBr	0.1132
$MnCl_2.4H_2O$	0.0002
H_3BO_3	0.7778
KCl	0.175
$MgCl_2.6H_2O$	0.9199
$CaCl_2.2H_2O$	0.3851
NaCl	10.3322
NaH_2PO_4	0.0063
Na_2SO_4	0.003

Footnote: Si was added as a 1000 mg l^{-1} Si standard final [Si] = 25 mg l^{-1}.

Sodium acetate ($CH_3.COONa.3H_2O$) was added at 0.25 g l^{-1}.

Table 2. Mean total counts of bacteria in the biotic column as determined by epifluorescence microscopy

Outflow fluid bacteria ml^{-1}	**Standard error**	**Comments**
0	n/a	Outflow (start up fluid)
0	n/a	Outflow prior to inoculation
0	n/a	7 days after inoculation
$8.64x10^5$	$6.68x10^4$	14 days after inoculation
$5.11x10^5$	$4.3x10^4$	21days after inoculation
$4.48x10^5$	$7.07x10^4$	28 days after inoculation

Table 3. Quantitative bulk XRD analysis. Crystalline mineralogy in wt.%.

Mineral	**Original core**		**Post-experimental**	
	(40 m)	**(90 m)**	**(biotic)**	**(abiotic)**
Albite	20	19.6	20.1	19.3
Chlorite	2.6	1.9	1.6	1.9
Halite	<0.5	<0.5	0.9	1.6
'Kaolin'	2.1	2.9	2.3	2.5
K-feldspar	8.7	7.4	8.6	7.2
'Mica'	22.1	21.8	21.3	21.8
Pyrite	2.4	2.9	2.1	2.3
Quartz	39.2	40.4	40	40.8
Smectite	2.9	3.1	3.1	2.6

Footnote: KEY: 'mica' = undifferentiated mica species including muscovite, biotite, illite and illite/smectite etc. 'kaolin' = one of the kaolinite group minerals including halloysite, kaolinite etc.

Table 4. Summary of BET/nitrogen surface area analyses

Sample description	**Surface area (m^2 g^{-1})**
Original core at 40 m	21.88
Original core at 90 m	24.07
Post experimental material (biotic)	22.08
Post experimental material (abiotic)	24.42